Study of harmonic site position variations determined by very long baseline interferometry

Leonid Petrov

NVI Inc./NASA Goddard Space Flight Center, Greenbelt, Maryland, USA

Chopo Ma

NASA Goddard Space Flight Center, Greenbelt, Maryland, USA

[1]   Position variations of 40 very long baseline interferometry (VLBI) stations at 32 tidal frequencies were obtained from analysis of 3 million measurements of group delays from 1980 to 2002. Residual displacements after the removal of the effect of solid Earth tides were studied. The purpose of this study is to investigate a harmonic signal at any frequency where it is expected and to assess quantitatively whether the models of vertical and horizontal site position variations agree with the observations. It was found that the estimates of station displacements are generally in good agreement with the ocean loading computed on the basis of ocean tide models for the main diurnal and semidiurnal tides. Moreover, VLBI results allow us to discriminate between different ocean tide models. However, discrepancies between VLBI results and all models of ocean loading for K_1, K_2, and S_2 tides exceed both the errors of the VLBI estimates and the errors of ocean loading displacements based on the reported formal uncertainties of ocean tide models. It was found that there is a significant nontidal signal at diurnal and annual frequencies. Applying a model of hydrological loading reduces the variance of the residual vertical displacements at the annual frequency by 30%. Using an empirical model of harmonic site position variations in VLBI processing provides a better fit and improves the baseline length repeatability.   *INDEX TERMS:* 1229 Geodesy and Gravity: Reference systems; 1249 Geodesy and Gravity: Tides—Earth; 4560 Oceanography: Physical: Surface waves and tides (1255); *KEYWORDS:* ocean, tide, loading, VLBI

1. Introduction

[2] Advances in space geodesy over the last two decades have allowed us to measure directly not only secular motion caused by tectonic processes, but also periodic displacements at timescales from hours to years caused by tides and various mass loadings. Periodic deformation of the Earth surface was first revealed indirectly as the factor which leads to a lengthening of the period of free wobble [*Newcomb*, 1892]. In the early 1980s, displacements caused by solid Earth tides were measured directly [*Ryan et al.*, 1986; *Herring et al.*, 1983] and these measurements provided estimates of Love numbers, which were close to theoretical values. Later these estimates were refined [*Mitrovica et al.*, 1994; *Ray et al.*, 1995; *Haas and Schuh*, 1996, 1998; *Wu et al.*, 2001]. The first evidence that displacements due to loading caused by ocean tides noticeably affect observations was obtained by *Schuh and Moehlmann* [1989]. The amplitudes and phases of radial displacements due to ocean loading for some selected stations were obtained by analyzing very long baseline interferometry (VLBI) [*Sovers*, 1994; *Haas and Schuh*,

1998; *Scherneck et al.*, 2000], SLR [*Christodoulidis et al.*, 1986; *Gendt and Dietrich*, 1986], and GPS data [*Lambert et al.*, 1998; *Dragert et al.*, 2000; *Schenewerk et al.*, 2001; *Hatanaka et al.*, 2001]. Displacements due to atmosphere pressure loading were detected from analysis of VLBI [*MacMillan and Gipson*, 1994; *van Dam et al.*, 1994] and GPS data [*van Dam et al.*, 1994]. Recently, evidence was found that displacements due to hydrology loading caused by seasonal changes of groundwater level and soil moisture agree with results of GPS measurements for at least some stations [*van Dam et al.*, 2001].

[3] Thorough analysis of VLBI results indicates that some effects are not modeled properly. It is known that series of baseline lengths exhibit seasonal variations [*Titov and Yakovleva*, 1999] For some baselines, like NRAO20/WETTZELL (Figure 1), these variations can be clearly seen. Earth orientation parameters (EOP) determined at simultaneously running VLBI networks do not agree within reported formal uncertainties [*MacMillan and Ma*, 2000] and show a pattern of differences (Figure 2). These examples suggest that VLBI observations are sensitive enough to detect the presence of signals, which are either not modeled or modeled incorrectly. This forces us to look critically at the models of periodic changes of site positions.
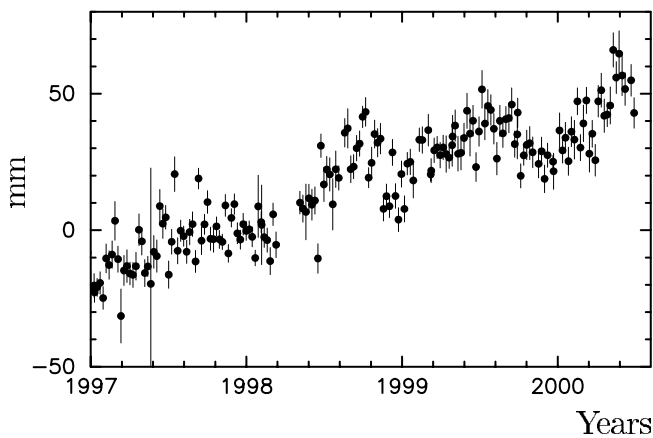
Figure 1. Time series of the length of transatlantic baseline NRAO20/WETTZELL determined by VLBI.

[4] While station displacements caused by four geophysical effects, solid Earth tides and pole tide, ocean loading, atmosphere loading and hydrology loading, were detected by space techniques, and they were found qualitatively in agreement with theoretical models, only the first effect was studied quantitatively in detail. Recently, *Schenewerk et al.* [2001] determined the amplitudes and phases of eight major diurnal and semidiurnal constituents of radial displacements caused by ocean loading for 353 stations using 3 years of GPS data. That paper gave us a quantitative insight on how well our models of ocean loading perform globally, not only for a specific site of interest, and pointed at the systematic differences between the obtained signal and models. Motivated by these results we expand this approach to a VLBI data set and study a harmonic signal at any frequency where it can be expected.

[5] In this paper the amplitudes and phases of three-dimensional harmonic site position variations were determined from analysis of all available VLBI data. The purpose of the study was to answer the questions

 1. Do current models of ocean loading quantitatively agree with observations?

 2. Can VLBI data discriminate between different ocean tide models?

 3. What is the best strategy for modeling minor tides? Is the procedure of admittance interpolation adequate?

 4. Are nontidal site position variations significant? Do they correspond to some geophysical phenomenon or rather an artifact?

 5. Does applying an empirical model of harmonic variations of site positions improve the accuracy of VLBI results: baseline length repeatability and consistency between results at simultaneous networks?

[6] The data set used in the analysis is described in section 2. Section 3 discusses details of the data analysis technique. In section 4, results are evaluated and compared with theoretical models. Concluding remarks are given in section 5. Algorithms used for computation of the displacements caused by solid Earth tides are given in appendices.

2. Observations

[7] All dual-band Mark-3/Mark-4/K-4 VLBI observations carried out under various geodetic and astrometric programs from 1979 are available on-line at the IVS Data Centers at http://ivscc.gsfc.nasa.gov [*Vandenberg*, 1999]. The VLBI data set has substantial spatial and time inhomogeneity. Typically, observations are made in sessions with a duration of about 24 hours. Observations were sporadic in the early 80s, but in January 1984 a regular VLBI campaign for determination of the EOPs started first with 5-day intervals, from May 1993 with weekly intervals, and then from 1997 twice per week. In addition to the observations dedicated to the EOP measurements, various other observing campaigns were running. Between 100 and 200 daily sessions per year were observed since 1984.

[8] In total, 141 stations participated in observations, although a majority of them observed only during short campaigns. The stations which participated in more than 20,000 observations for more than 3 years were used for analysis. Forty-six stations satisfied these criteria. Four stations which participated in the KSP project [*Takahashi et al.*, 2000], KASHIM11, KOGANEI, MIURA, and TATEYAMA, were excluded since they observed mainly in a small local network as well as two other stations, CRIMEA since prior 1998 it had known problems with equipment [*Petrov et al.*, 2001], and YLOW7296 since its sensitivity is too low. Only observations at the baselines between these 40 strong selected stations were used, other observations (∼6%) being discarded. Sessions with less than 3 strong stations were discarded entirely. 3126 sessions from April 1980 to January 2002 with more than 3 million observations remained, and they were used in the analysis.

[9] The number of participating stations in each individual session varies from 2 to 20, although 4–7 is a typical number. No station participated in all sessions, but every station participated in sessions with many different networks. All networks have common nodes and therefore, are tied together. Networks vary significantly, but more than 70% of them have a size exceeding the Earth's radius.

[10] From 10 to 116 sources, radiogalaxies or quasars with flux density 0.2–10 Jy, are observed in each session. The data set used in the analysis contains observations of 701 quasars. Like stations, no source was observed in every session, many of the sources were observed only occasionally, and 100 of the most frequently observed sources yielded 92% of the data. The pool of sources has a core
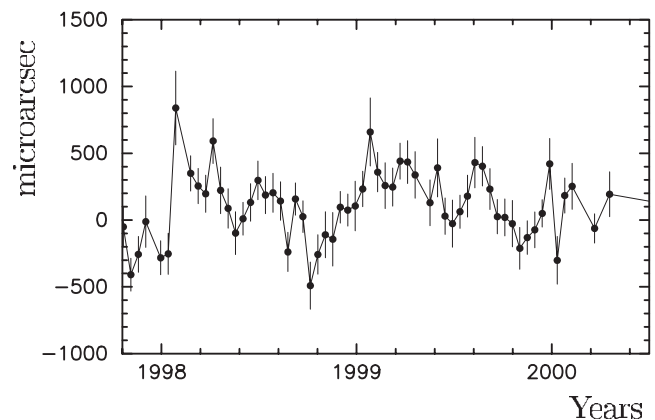
Figure 2. Differences in *X* pole coordinates determined from VLBI observations at the simultaneously running independent networks, CORE-A and NEOS-A.

subset, which was changed by adding or removing some sources occasionally, 2–3 times per year. These core sources connect networks between sessions. Although radiogalaxies and quasars are located at distances on the scale of gigaparsecs, an initial analysis showed that a considerable portion of them, 25%, exhibits apparent proper motion, probably caused by changes in their structure.

[11] During a session antennas observe a sequence of sources. A station tracks a source for 30–600 s and then immediately slews to another source. The observing schedule is optimized to provide sky coverage as uniform as possible. Every hour several sources at elevations 5°–20° are added to the schedule. A typical schedule allows us to obtain reliable station positions using 3–5 hours of observations.

3. Data Analysis

[12] Data analysis is comprised of a computation of theoretical delays, weighted least squares (LSQ) fit of parameter adjustments of a model to the small differences between observed and theoretical delays, a transformation of the set of adjustments of the station position variations, and then a comparison of the results with theoretical values.

3.1. Theoretical Model

[13] Computation of theoretical time delays in general follows with some exceptions the procedure outlined in the IERS Conventions [McCarthy, 1996] and described in more detail by Sovers et al. [1998]. No model was applied for ocean loading, atmosphere pressure loading, or high frequency EOP. The IERS96 semiempirical nutation expansion was used. Displacement of the reference point of a VLBI station due to thermal expansion of the antenna was not modeled. Although there were attempts to measure it directly at several antennas [Zernecke, 1999] and to develop a model [Nothnagel et al., 1995], this model was not yet validated.

[14] It was found that the approximate expression for displacements due to solid Earth tides introduced by Mathews et al. [1997] and adopted in the IERS Conventions does not provide the targeted precision of 0.1 mm. Instead of expressing solid Earth tides in the time domain using ephemerides and applying numerous corrections, displacements due to solid Earth tides were sought in the frequency domain [Buellesfeld and Schuh, 1986].

[15] The most complete tidal catalogue, HW95 [Hartman and Wenzel, 1995], was used for computations. However, there is no need to take into account all 12,935 waves from that catalogue. Since the expected formal uncertainties of the estimates of radial displacements for a harmonic signal at the semidiurnal band are 0.3 mm, the cutoff for computations of solid Earth tides is chosen at 0.1 mm. It means that the tide-generating potential of the second degree should be computed with a relative precision of 2×10^{-4}, and the potential of the third degree with a precision of only 5×10^{-2}. This requirement for precision allows us to neglect mixed terms of the form $t \sin \omega t$, neglect terms in the arguments for expansion proportional to the second and higher order in time and substantially reduce the total number of constituents. Direct comparison of the time series of the tide-generating potential computed for the time

interval 1980–2020 using the simplified expansion, which contains 550 purely harmonic terms of the second degree as well as 50 terms of the third degree with the largest amplitudes, and the series produced using the complete original HW95 catalogue showed that the RMS of the differences in radial displacements did not exceed 0.1 mm. This cutoff limit does not mean that we believe that the solid Earth tide model is accurate at the level of 2×10^{-4}, but at least we can be sure that omitted terms do not produce an error comparable with the formal uncertainties of the phenomena under consideration. Displacements caused by the solid Earth tides can be written elegantly through the frequency-dependent generalized Love numbers using the spectrum of the tide-generating potential as is shown in the appendix. Numerical values for generalized Love numbers for diurnal tides were given by Mathews [2001] and for zonal and semidiurnal tides by Mathews et al. [1997].

3.2. Estimation Model

[16] Estimated parameters were split into two classes: basic parameters, which are usually adjusted for processing VLBI experiments, and specific parameters of interest. Basic parameters belong to one of the three groups:

1. *global* (over the entire data set): positions and velocities of 40 stations, positions of 414 primary sources, proper motion of 79 sources.

2. *local* (over each session): pole coordinates and their rates, UT1, UT1 rate; positions of other sources, atmosphere gradients for all stations and their rates, station-dependent clocks modeled by second-order polynomials, baseline-dependent clock offsets.

3. *segmented* (over 0.33–1.0 hours): coefficients of a linear spline atmospheric path delay (0.33-hour segment) and for clock function (1-hour segment) for each station. The estimates of clock function absorb uncalibrated instrumental delays in the data acquisition system.

[17] The rate of change of atmospheric path delay and clock function between two adjacent segments was constrained to zero with weights reciprocal to 40 ps/hour and 2×10^{-14} s/s, respectively, in order to stabilize the solution.

[18] When we solve for the positions of all of the stations and sources as well as for the EOPs, we should take into account the fact that not all parameters are linearly independent. An approximate expression for the time delay, τ, of a two-element radio interferometer is given by

$$\tau = \frac{1}{c}\widehat{\mathcal{D}}(\vec{r}_1 - \vec{r}_2)\widehat{\mathcal{P}}\,\vec{s} \qquad (1)$$

where c denotes the speed of light in a vacuum, $\vec{r}_i$ is the vector of station coordinates, $\vec{s}$ is the vector of source coordinates, $\widehat{\mathcal{D}}$ and $\widehat{\mathcal{P}}$ are the matrices of diurnal rotation and precession-nutation.

[19] It is clear that if an arbitrary vector is added to all of the site positions, the value of the time delay remains the same. If all of the vectors of site positions are rotated by an arbitrary vector of a small rotation, and the matrix $\widehat{\mathcal{D}}$ is multiplied by the inverse of the rotation matrix which corresponds to this vector, which will be equivalent to adding a constant to pole coordinates and UT1, the time delay remains the same. Analogous arguments are valid for the time derivative of site

positions and $\widehat{\mathcal{D}}$ as well as for source coordinates and the matrix $\widehat{\mathcal{P}}$.

[20] Since the equation for the time delay is invariant with respect to a 15-parameter linear transformation, including a translation and a rotation of station coordinate vectors and their time derivatives as well as a rotation of source coordinate vectors, the resulting normal matrix is rank deficient. In order to solve a rank deficient LSQ problem, the following constraints on global parameters are imposed: net-rotation constraints on station positions, station velocities, source coordinates; net-translation constraints on station positions and velocities.

[21] Constraint equations for net translation and net rotation are written in the form:

$$
\begin{aligned}
\sum_i \Delta \vec{P}_i &= \text{const} \\
\sum_i \frac{1}{r_i^2} \Delta \vec{P}_i \times \vec{r}_i &= \text{const}
\end{aligned}
\tag{2}
$$

where $\Delta \vec{P}$ is a vector of the estimates of station position or velocity, $\vec{r}$ is a vector of station coordinates, and the summing is done over all stations. The constants in the right hand side of (2) were set to zero.

[22] Parameters of interest for this study included sine and cosine coefficients of harmonics of the spectrum of site position. Since it is not feasible to estimate site position variations at all spectral constituents, some selection should be done on the basis of the expected spectrum of station displacements. It was assumed that the main spectral constituents should correspond to the principal tidal lines, as well as to the annual and diurnal variations (period of one *solar* day) and their multiple harmonics. The rationale for including tidal constituents is to try to capture variations caused by ocean loading and deficiencies in the solid Earth tide model. Harmonics of annual variations were included in an attempt to capture seasonal variations caused by nontidal loading. Harmonics of diurnal variations as well as the ψ_1, φ_1 tidal waves were included because they have a reputation of "dirty" spectral lines where some unexpected phenomena may occur; e.g., *Rothacker et al.* [2001] reported that analysis of GPS data showed significant variations in the Earth's rotation at the set of multiple harmonics of the diurnal frequency. Since for every frequency of interest we can find a constituent in the spectrum of the tide-generating potential, all of them will be later called as tidal waves, although a direct tidal displacement for some of them is negligible. In addition to the frequencies at which we can expect variations in site positions, several tidal waves at which we do not expect any signal were included in order to give us an estimate of the accuracy of the results.

[23] One of the complications in estimating site position variations at tidal frequencies is that the spectrum of the tide-generating potential has close spectral lines. Some of them are separated by the frequency which corresponds to a period of 18.6 years, and these constituents cannot be resolved for a majority of stations since they did not observe long enough. Therefore, we must use some a priori information. It was assumed that within a narrow frequency band the phase lag of the displacement is constant, and the ratio of the amplitudes of displacements is the same as the ratio of the amplitudes of the tide-generating potential. The basis of this assumption is the fact that the ocean response to the

tide-generating potential is a localized function of time; therefore its Fourier transform is a relatively smoothly varying function of frequency [*Gipson*, 1996]. The tides within a narrow band were combined into a group. Instead of estimating the amplitudes and phases of each component of the group, which is impossible, the admittance of the entire group was estimated.

[24] 6 parameters of station displacements were estimated for each frequency group. Their dependence on time is given by

$$
p_j^c = \sum_k \frac{A_k}{A_o} \cos \left(\psi_k + \theta_k + \omega_k t_{\text{TDB}} + m_k \frac{2\pi(\text{UT1} - t_{\text{TDB}})}{86400} \right)
$$
$$
p_j^s = \sum_k \frac{A_k}{A_o} \sin \left(\psi_k + \theta_k + \omega_k t_{\text{TDB}} + m_k \frac{2\pi(\text{UT1} - t_{\text{TDB}})}{86400} \right)
\tag{3}
$$

where the index j ranges over the X, Y, and Z components in the geocentric system, A_k stands for the amplitude of the tide-generating potential for the kth tidal wave of the group, A_o stands for the amplitude of the principle term of the group, ψ_k is the phase of the tide, θ_k and ω_k are the phase and the frequency of the argument of the tide-generating potential expansion, m_k is the order of the tidal wave, and t_{tdb} is the time elapsed since the fundamental epoch J2000.0 (12^h 1 January 2000) at the TDB scale. The frequency ranges of the tidal groups used for estimation of site displacements and the amplitudes of the tide-generating potential of the main component of the tidal waves are listed in Table 1.

[25] We found previously that equation for time delay (1) is invariant with respect to a six-parametric linear transformation of site positions. Vectors of harmonic site position variation $\vec{p^c} = a\,\vec{r}\cos(\alpha)$ and $\vec{p^s} = b\,\vec{r}\sin(\alpha)$ inherit this property. It is obvious that if an arbitrary vector is added to all vectors $\vec{p^c}$ or $\vec{p^s}$, the time delay remains the same since only a difference of coordinates enters into (1). If a small rotation is applied to all vectors $\vec{p^c}$ or $\vec{p^s}$, and retrograde and prograde variations of the EOPs at the same frequency are applied, the time delay remains the same. Daily estimates of pole coordinates and UT1 will almost entirely absorb harmonic variations with long periods, $P \gg 1^d$, and therefore, a small net rotation of vectors $\vec{p^c}$, cannot be distinguished from a sinusoidal variation of the daily estimates of the EOPs. It is known that the Earth orientation variations with $P \leq 1^d$ periods are significant [*Gipson*, 1996]. We cannot use theoretical values for them in this study because, first, theoretical models are not yet sufficiently precise, and second, the number of stations is relatively small, 40, and their distribution is not uniform. Therefore, the difference between the net rotation of the vectors of the harmonic variation of the position of these sites and the harmonic variation in the rotation of the deformable Earth at this frequency as a whole obtained by integrating over the surface of the Earth is not necessarily negligible. For these reasons variations of polar motion and UT1 at the targeted frequencies, except the frequencies of zonal tides, were added to the list of estimated parameters. The set of estimated high frequency EOPs included parameters that are equivalent to celestial pole offsets, precession rate and several main nutation constituents, except the principal

Table 1. Amplitudes and Frequencies of Tidal Groups Used in Parameter Estimation

Wave	Doodson Argument	Frequency Range (rad/s)	Amplitude (m^2/s^2)
S_4	491.555	$(2.9088-2.9089) \times 10^{-4}$	0.00000
M_4	455.555	$(2.8103-2.8104) \times 10^{-4}$	0.00097
S_3	382.555	$(2.1816-2.1817) \times 10^{-4}$	0.00009
M_3	355.555	$(2.1077-2.1078) \times 10^{-4}$	0.07504
–	295.355	$(1.5117-1.5118) \times 10^{-4}$	0.00359
K_2	275.555	$(1.4583-1.4587) \times 10^{-4}$	0.78303
S_2	273.555	$(1.4544-1.4545) \times 10^{-4}$	2.88175
T_2	272.556	$(1.4524-1.4525) \times 10^{-4}$	0.16824
L_2	265.455	$(1.4315-1.4321) \times 10^{-4}$	0.17511
M_2	255.555	$(1.4050-1.4052) \times 10^{-4}$	6.19455
ν_2	247.455	$(1.3822-1.3824) \times 10^{-4}$	0.22530
N_2	245.655	$(1.3786-1.3788) \times 10^{-4}$	1.18605
μ_2	237.555	$(1.3558-1.3560) \times 10^{-4}$	0.18943
$2N_2$	235.755	$(1.3522-1.3525) \times 10^{-4}$	0.15695
OO_1	185.555	$(7.8244-7.8266) \times 10^{-5}$	0.11051
–	115.855	$(5.9680-5.9681) \times 10^{-5}$	0.00732
J_1	175.455	$(7.5549-7.5572) \times 10^{-5}$	0.20204
φ_1	167.555	$(7.3319-7.3320) \times 10^{-5}$	0.05133
ψ_1	166.554	$(7.3120-7.3121) \times 10^{-5}$	0.02865
K_1	165.555	$(7.2910-7.2943) \times 10^{-5}$	3.61208
S_1	164.556	$(7.2722-7.2723) \times 10^{-5}$	0.02864
P_1	163.555	$(7.2512-7.2523) \times 10^{-5}$	1.19331
M_1	155.655	$(7.0281-7.0293) \times 10^{-5}$	0.20197
O_1	145.555	$(6.7576-6.7598) \times 10^{-5}$	2.56942
ρ_1	137.455	$(6.5301-6.5312) \times 10^{-5}$	0.09338
Q_1	135.655	$(6.4947-6.4959) \times 10^{-5}$	0.49195
-	0A3.455	$(1.2887-1.2888) \times 10^{-5}$	0.00482
Mtm	085.455	$(7.9626-7.9841) \times 10^{-6}$	0.12496
Mf	075.555	$(5.2784-5.3449) \times 10^{-6}$	0.65263
Mm	065.455	$(2.6285-2.6950) \times 10^{-6}$	0.34474
Ssa	057.555	$(3.9821-4.0891) \times 10^{-7}$	0.30312
Sa	056.554	$(1.9909-1.9910) \times 10^{-7}$	0.04888

nutation term. In order to compensate for this omission, additional parameters, which are equivalent to retrograde and prograde nutation with period of 18.6 years, were added to the list of estimated parameters.

[26] Since atmosphere pressure loading was not modeled, parameters of pressure loading admittance were estimated for each station in the same manner as was done by *MacMillan and Gipson* [1994]: $u_v = A \cdot P$ where u_v is a vertical displacement, P is local atmosphere pressure and A is an admittance parameter. Although it is known that this model is too simple [*van Dam and Wahr*, 1987], it should account for 10–80% of the signal computed from the full convolution model.

[27] Estimation of harmonic site position variations increases the rank deficiency of the normal matrix. In order to eliminate the rank deficiency, equations of constraints in the form of (2) were applied for the sine and cosine components of site variations for each wave. The arbitrariness of the constants in the right hand side of equations of constraint means that we cannot determine exact amplitudes and phases of harmonic variations from analysis of observations, but are able to determine only a family of solutions. In order to pick up a specific element from this family, we have to specify boundary conditions using some additional information. The following strategy was chosen: first make a solution with constraints in the simplest form, setting the constants in the right parts to zero, then later determine the parameters of a linear transformation, translation and rotation, for the sine and cosine components for each wave from boundary conditions, and then finally apply these transformations.

[28] Thus, four groups of parameters of interest were estimated in the solution called H1: (1) sine and cosine components for three-dimensional site position variations for all stations, 32 tidal waves; (2) variations of polar motion and UT1 at these tidal waves, except the waves with periods longer than 3 days, since they are absorbed in the estimation of the EOPs for each session; (3) principal nutation terms; and (4) admittance of atmosphere pressure loading. All these parameters are considered as global. More than 1.4 million parameters, including 9000 global, were adjusted by solving the weighted LSQ problem with minimal constraints of the form (2) in a single solution.

3.3. Boundary Conditions

[29] Now we search for the boundary conditions that allow us to define the parameters of the invariant transformation, translation and rotation, for the obtained field of harmonic site displacements. It is desirable to avoid setting the harmonic variations of position of some stations to theoretical values, since the errors in the theoretical model would propagate to displacements of other stations which would make comparison with theoretical models difficult.

[30] We should be aware that the choice of specific boundary conditions affects the separation of vertical site position variations from horizontal. Figure 3 illustrates it. However, this property can be used for defining boundary conditions. In general, all loading effects cause vertical displacements at least 3 times greater than horizontal displacements. Therefore, the vertical component of the displacement should dominate the horizontal one. Thus, the boundary condition which defines parameters of the invariant transformation in such a manner that the weighted sum of squares of the horizontal displacements after the transformation will be at a minimum has a clear physical meaning: it makes the field of displacements consistent with the field caused by mass loading. Parameters of the invariant transformation are found by weighted LSQ.

[31] We can write the transformation of the vector of harmonic station position variations of the ith station in the form $\vec{u}_{ni} = \vec{u}_i + \widehat{\mathcal{M}}_i \vec{\xi}$ where $\vec{u}_i$ is the sine or cosine vector of observed harmonic station displacements in the geocentric reference frame, $\vec{u}_{ni}$ is this vector after transformation, $\vec{\xi}$ is the unknown six-dimensional vector of the invariant transformation and $\widehat{\mathcal{M}}_i$ is the matrix of this transformation for the ith station:

$$\widehat{\mathcal{M}}_i = \begin{pmatrix} 1 & 0 & 0 & 0 & r_3 & -r_2 \\ 0 & 1 & 0 & -r_3 & 0 & r_1 \\ 0 & 0 & 1 & r_2 & -r_1 & 0 \end{pmatrix} \qquad \vec{\xi} = \begin{pmatrix} T_1 \\ T_2 \\ T_3 \\ \Omega_1 \\ \Omega_2 \\ \Omega_3 \end{pmatrix} \qquad (4)$$

where r_k are the components of the station geocentric coordinates, T_k and Ω_k are the components of the vector of a translation and a small rotation respectively.

[32] The transformed vector of the topocentric harmonic site position variations vanishes when

$$\widehat{\mathcal{H}}_i \widehat{\mathcal{M}}_i \vec{\xi} = -\widehat{\mathcal{H}}_i \vec{u}_i \qquad (5)$$

where $\widehat{\mathcal{H}}_i$ is the transformation matrix from the geocentric to the topocentric reference frame.

a)   b)
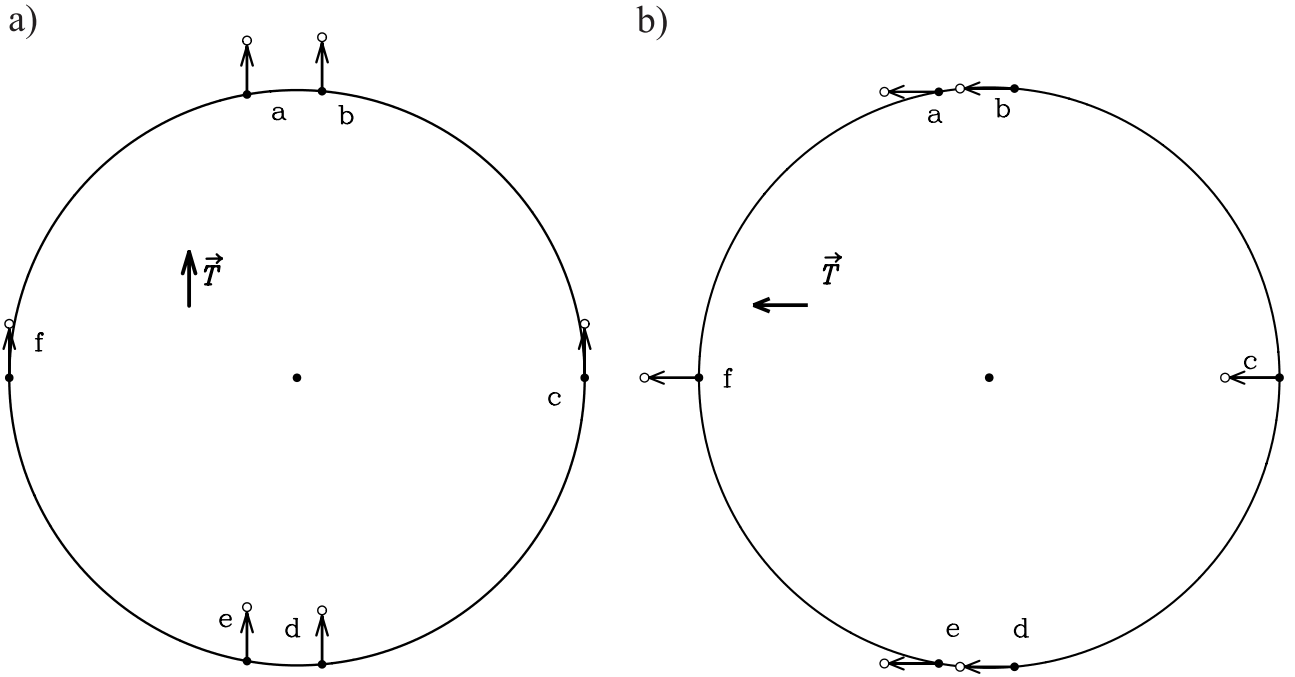
Figure 3. Effect of changes of boundary conditions on the separation of horizontal and vertical components of displacement. (a) Points a, b, e, and d have vertical motion and points c and f have horizontal motion. (b) Changes in boundary conditions resulted in changes of the translation vector $\vec{T}$ and caused points c and f to have only vertical motion, while points a, b, e, and d have only horizontal motion.

[33] In general, the estimates of harmonic site positions are not statistically independent, but analysis of the covariance matrix showed that only correlations between displacements which correspond to the same station and the same tidal wave are significant, other correlations being by absolute value less than 1×10^{-4}. Thus, parameters of the invariant transformation can be obtained for each wave separately. At the same time parameters of the transformation for sine and cosine components for each tidal wave should be obtained in a combined solution. To make a combined solution we merge vectors $\vec{\xi^c}$ with $\vec{\xi^s}$, $\vec{u^c}$ with $\vec{u^s}$ and expand matrices $\mathcal{H}_i$, $\mathcal{M}_i$:

$$\widehat{\mathcal{H}}_i^* = \begin{pmatrix} H_i & 0 \\ 0 & H_i \end{pmatrix} \qquad \widehat{\mathcal{M}}_i^* = \begin{pmatrix} M_i & 0 \\ 0 & M_i \end{pmatrix}$$
$$\vec{\xi}^* = \begin{pmatrix} \xi^c \\ \xi^s \end{pmatrix} \qquad \vec{u}_i^* = \begin{pmatrix} u_i^c \\ u_i^s \end{pmatrix} \qquad (6)$$

[34] Then we can find values of a 12-dimensional vector $\vec{\xi}^*$ by solving the system of linear equations $\sum_i \widehat{\mathcal{H}}_i^* \widehat{\mathcal{M}}_i^* \vec{\xi}^* = -\sum_i \widehat{\mathcal{H}}_i^* \vec{u}_i^*$ by LSQ with the full weight matrix

$$\widehat{W} = \widehat{\mathcal{R}} \left(\widehat{\mathcal{H}}^{*\top} \mathrm{Cov} \left(\vec{u}_i^*, \vec{u}_i^{*\top} \right) \widehat{\mathcal{H}}^* \right)^{-1} \qquad (7)$$

where $\widehat{\mathcal{R}}$ is a diagonal matrix with 1 for the elements which correspond to horizontal components and 0.01 for the elements which correspond to vertical components. Very small relative weights for vertical components of the displacements field in the fudge matrix $\widehat{\mathcal{R}}$ effectively exclude vertical components in the minimization process.

[35] After applying the transformation $\vec{u_{ni}} = \vec{u}_i + \widehat{\mathcal{M}}_i \vec{\xi}$ for each tidal wave we get the final field of harmonic site position variations.

3.4.   Error Analysis

[36] Each value of group delay is computed using about 10^9 bits of information [*Clark et al.*, 1985]. This redundancy allows us to evaluate an uncertainty of each observation that depends on the sensitivity of the antennas, source flux density and other factors. Since formal uncertainties of group delay measurements vary at 2 orders of magnitude, proper weighting is essential. In order to take into account unmodeled effects, mainly instrumental phase noise and mismodeling troposphere path delay, for each session and each baseline additive corrections to formal uncertainties were computed during preliminary analysis in such a manner that the ratio of the weighted sum of squares of residuals to its mathematical expectation is close to unity. Despite of all these precautions, the errors derived from these formal uncertainties through the error propagation law are still underestimated. Numerous tests, such as a decimation test and analysis of results from close stations, and analysis of results at simultaneously running VLBI networks showed [*Ryan et al.*, 1993] that the uncertainties of station velocities, EOP series and other parameters obtained by weighted LSQ should be scaled by a factor of 1.1–1.6. One of the possible reasons for this deficiency in the error model is unaccounted correlations between delays at the baselines with a common station.

[37] In order to find these multiplicative reweighting parameters, the estimates of harmonic variations at the frequencies where no tidal effect is expected were obtained. For each wave the weighted χ^2 per degree of freedom

Table 2. Accuracy of Determination of Harmonic Site Position Variations in mm

Station	Long Period			Diurnal Band			Semidiurnal Band		
	Up	East	North	Up	East	North	Up	East	North
ALGOPARK	1.6	0.5	0.5	0.8	0.3	0.3	0.8	0.2	0.3
BR-VLBA	2.3	0.5	0.5	1.4	0.2	0.4	1.2	0.3	0.3
DSS45	3.7	1.2	2.9	3.6	1.3	1.5	2.0	0.7	0.7
DSS65	5.3	0.8	1.4	2.7	0.6	0.7	2.6	0.6	0.5
FD-VLBA	1.8	0.4	0.4	1.2	0.2	0.2	1.0	0.3	0.3
FORTLEZA	1.7	0.8	0.5	1.1	0.4	0.3	0.8	0.4	0.4
GILCREEK	0.9	0.4	0.4	0.5	0.2	0.2	0.4	0.1	0.1
HARTRAO	1.8	1.2	1.4	1.7	0.8	1.0	1.3	0.5	0.7
HATCREEK	6.8	1.3	1.6	3.1	0.9	0.8	2.1	0.8	0.7
HAYSTACK	6.7	1.8	2.1	3.3	1.3	1.3	2.4	0.9	1.1
HN-VLBA	3.4	0.6	0.8	2.4	0.6	0.4	1.8	0.2	0.4
HOBART26	3.5	1.8	2.2	2.2	0.8	1.3	1.7	0.6	0.8
HRAS-085	4.9	1.4	1.5	1.0	0.3	0.4	0.7	0.3	0.4
KASHIM34	7.2	2.3	1.8	5.2	1.4	1.5	3.5	0.9	1.4
KASHIMA	4.3	1.6	1.6	2.5	0.6	0.9	1.6	0.5	0.7
KAUAI	2.5	1.3	1.4	2.0	0.6	0.7	1.0	0.5	0.4
KOKEE	1.4	0.5	0.8	0.7	0.3	0.4	0.8	0.4	0.3
KP-VLBA	2.7	0.4	0.6	1.5	0.3	0.3	1.6	0.3	0.3
LA-VLBA	1.7	0.4	0.3	1.0	0.3	0.2	0.9	0.2	0.2
MATERA	1.6	0.3	0.5	1.1	0.3	0.3	0.9	0.2	0.3
MEDICINA	1.4	0.5	0.5	1.0	0.3	0.3	1.0	0.3	0.2
MK-VLBA	3.3	0.8	0.6	1.4	0.4	0.4	1.2	0.3	0.4
MOJAVE12	1.5	0.7	0.7	0.6	0.4	0.2	0.6	0.2	0.3
NL-VLBA	3.0	0.5	0.6	0.8	0.3	0.2	1.4	0.2	0.2
NOTO	2.9	1.1	1.0	1.7	0.4	0.6	2.2	0.6	0.7
NRAO20	2.8	0.6	0.6	1.0	0.3	0.4	1.0	0.2	0.3
NRAO85-3	2.5	1.1	0.5	0.8	0.4	0.2	0.9	0.2	0.3
NYALES20	3.0	0.3	0.4	1.0	0.2	0.2	0.6	0.2	0.2
ONSALA60	1.4	0.3	1.1	1.3	0.2	0.3	1.2	0.2	0.3
OV-VLBA	2.7	0.6	0.6	1.6	0.3	0.2	1.2	0.3	0.3
OVRO-130	13.4	1.6	2.5	3.0	0.6	1.0	1.4	0.6	0.6
PIETOWN	4.2	0.6	0.6	1.1	0.2	0.3	0.9	0.2	0.3
RICHMOND	1.4	0.8	0.8	1.6	0.3	0.3	0.9	0.3	0.4
SANTIA12	7.4	2.7	2.6	3.8	1.2	1.6	1.9	1.2	0.8
SC-VLBA	4.9	1.1	0.8	2.9	0.6	0.6	1.9	0.6	0.7
SESHAN25	6.2	2.3	2.1	4.3	1.4	1.6	4.3	1.1	1.0
TSUKUB32	4.2	3.3	2.2	4.5	0.6	1.7	2.9	0.9	0.8
VNDNBERG	6.1	1.5	1.2	3.7	0.6	0.7	1.8	0.6	0.7
WESTFORD	1.4	0.5	0.4	0.6	0.2	0.2	0.5	0.2	0.1
WETTZELL	0.8	0.2	0.2	0.7	0.2	0.2	0.4	0.1	0.1

statistics were computed, separately for horizontal and vertical components:

$$\chi^2/\mathrm{ndg}(v) = \frac{\sum_{i}^{n} \widehat{\mathcal{H}}_i^* \vec{u}_i^* \widehat{\mathcal{H}}_i^{*\top} \left(\mathrm{Cov}\left(\vec{u}_i^*, \vec{u}_i^{*\top} \right) \right)^{-1} \widehat{\mathcal{H}}_i^* \vec{u}_i^{*\top} \widehat{\mathcal{H}}_i^{*\top} \widehat{\mathcal{R}}_v}{2n}$$

$$\chi^2/\mathrm{ndg}(h) = \frac{\sum_{i}^{n} \widehat{\mathcal{H}}_i^* \vec{u}_i^* \widehat{\mathcal{H}}_i^{*\top} \left(\mathrm{Cov}\left(\vec{u}_i^*, \vec{u}_i^{*\top} \right) \right)^{-1} \widehat{\mathcal{H}}_i^* \vec{u}_i^{*\top} \widehat{\mathcal{H}}_i^{*\top} \widehat{\mathcal{R}}_h}{4n}$$

(8)

where $\widehat{\mathcal{R}}_v$ is a diagonal matrix with 1 in the elements which correspond to vertical components and 0 for all others, and $\widehat{\mathcal{R}}_h$ is a diagonal matrix with 1 in the columns which correspond to horizontal components and 0 for all others. Sums are computed over all stations. If vectors $\vec{u}^*$ had only noise with zero mean and covariance $\mathrm{Cov}(\vec{u}_i^*, \vec{u}_i^{*\top})$, then the mathematical expectation of χ^2/ndg would be unity. Assuming that there is no signal at these frequencies, we multiply the covariance matrix by a fudge diagonal matrix in order to make χ^2/ndg unity. This rescaling increases formal uncertainties by the factors of $1.3-2.0$.

[38] Although estimation of site position variations at one frequency for each band where no signal is expected enables

us to compute reweighting parameters, this information is not sufficient to judge the accuracy of a determination of the signal at each individual station since the formal uncertainty of results varies for different stations by more than 1 order of magnitude. In order to evaluate the level of accuracy of results at each individual station, another solution, H2, was done with estimating harmonic site variations at 10 frequencies within each band: long period, diurnal and semidiurnal. These frequencies are selected to be away from tidal, diurnal and annual frequencies. By averaging the amplitudes of the obtained adjustments across each band we get the upper estimates for the accuracy of results. They are presented in Table 2. In contrast to formal uncertainties, which always are too low even after reweighting since correlations and possible systematic effects are ignored, these estimates give us the upper limit of accuracy since we ignored the possible presence of a real signal at those frequencies.

4. Discussion of Results

[39] The estimated amplitudes of harmonic site position variations are in the range of $1-30$ mm for vertical components, $1-10$ mm for horizontal components and substantially exceed the accuracy of their measurements
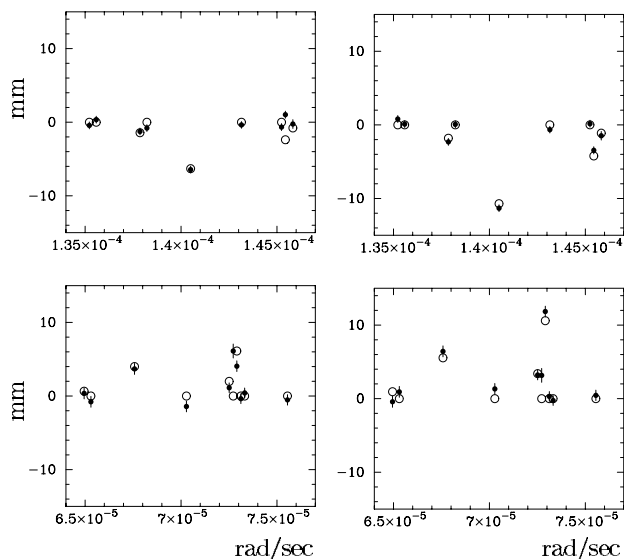
Figure 4. Real and imaginary parts of the vertical displacement of the KOKEE station at the semidiurnal and diurnal bands. The estimates of the displacements are shown by disks. Ocean loading computed using the NAO99 model is shown by circles.

at some frequencies. Figures 4 and 5 show an example of the empirical spectrum of site position variations and compare it with theoretical predictions. Figures for all other stations are available on the Web at http://gemini.gsfc.nasa.gov/harpos.

4.1. Ocean Loading Models for Major Tides

[40] The χ^2/ndg statistic was used as a measure of significance of the observed signal. The left columns of Table 3 show it for each wave. Assuming the distribution of the estimates of harmonic site position variations to be normal with zero mean and the variance obtained by rescaling formal uncertainties, we find from tables of χ^2 distribution that at the 95% confidence level the χ^2/ndg should be less than 1.25 for the vertical component and 1.19 for the horizontal component. Large values of the χ^2/ndg statistics for major tides shown in the left columns of Table 3 indicate the presence of statistically significant site position variations. Now we can try to compare the obtained signal with theoretical models.

[41] First consider ocean loading. Displacements of site positions due to ocean loading were computed using three different models of ocean tides: Schwiderski model [*Schwiderski*, 1980] based on a hydrodynamical interpolation and sea level measurements at coastal islands and deep-sea tidal gauge stations, and two models based on assimilation of sea surface height measurements by the Topex/Poseidon satellite altimeter and a hydrodynamic model: GOT00 [*Ray*, 1999] and NAO99 [*Matsumoto et al.*, 2000; *Takanezawa et al.*, 2001]. Displacements due to ocean loading were computed by the SPOTL program [*Agnew*, 1996, 1997] with Gutenberg–Bullen Green's functions [*Farell*, 1972].

[42] For comparison with ocean loading models, (5) for boundary conditions was slightly modified: the vector of site displacements computed by a model was added to its

right hand side, and the parameters of the transformation were found by minimizing the weighted sum of squares of the differences between observed and theoretical horizontal site position variations.

[43] Analysis of Table 3 shows that applying the models of ocean loading for the site position variations at the M_2, S_2, N_2, K_1, O_1, and P_1 frequencies helps to reduce residuals significantly. We can conclude that the largest portion of the observed signal is due to ocean loading.

[44] What can we learn from analysis of the residuals? The largest residual signals are at the annual and K_1, S_1, K_2, S_2 frequencies. Site position variations with periods of 1 year and one solar day (Sa and S_1) are, certainly, not related to astronomical tides since the corresponding amplitudes of the tide-generating potential are very small. We can suggest that observed variations may be due to changes in meteorological conditions. It is known that mismodeling of atmospheric path delay is a significant source of errors in VLBI [*Macmillan and Ma*, 1994]. Diurnal (S_1) and annual modulations of atmosphere modeling errors may cause a modulation in the final results at these frequencies. However, atmospheric mismodeling is usually detected by an elevation cutoff test, which exploits the fact that atmospheric modeling errors decrease rapidly with increasing elevation. Solution H3 was made with deleting the observations with an elevation below 15° at every station of a baseline, but site position variations changed only within rescaled formal uncertainties, and no significant change in χ^2/ndg was noticed. The hypothesis was not confirmed.

[45] Phasor diagrams for vertical and horizontal site position variations across North America are presented in Figure 6. Vertical site position variations show a pattern of spatial coherence, especially for the annual constituent, but the pattern of horizontal variations is rather chaotic. Since a
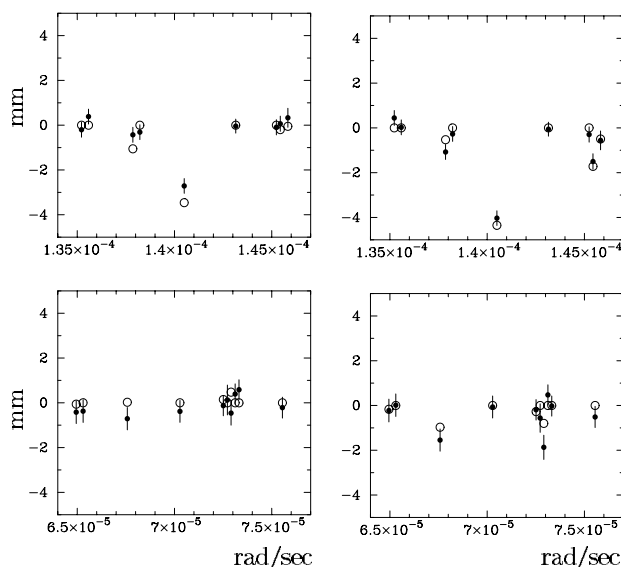
Figure 5. Real and imaginary parts of the north displacement of the FORTLEZA station at the semidiurnal and diurnal bands. The estimates of the displacements are shown by disks. Ocean loading computed using the NAO99 model is shown by circles.

Table 3. χ^2/ndg Statistic of Residual Harmonic Site Position Variations After Subtraction of Ocean Loading Models

Wave	No Model		Schwiderski		GOT00		NAO99	
	Vert	Horz	Vert	Horz	Vert	Horz	Vert	Horz
S_4	1.08	0.98	–	–	–	–	–	–
M_4	0.78	1.09	–	–	–	–	–	–
S_3	1.33	1.66	–	–	–	–	–	–
M_3	0.97	1.23	–	–	–	–	–	–
K_2	2.33	2.19	2.36	1.93	2.35	1.90	2.24	1.89
S_2	10.37	5.27	2.92	2.31	2.85	2.05	2.87	1.95
T_2	1.58	1.04	–	–	–	–	1.55	1.02
L_2	1.51	0.71	–	–	–	–	1.39	0.67
M_2	99.31	33.38	5.08	3.20	1.20	2.34	1.21	2.31
ν_2	1.17	1.30	–	–	–	–	1.05	1.15
N_2	6.13	2.60	1.73	1.20	1.80	1.18	1.81	1.18
μ_2	1.51	1.12	–	–	–	–	1.58	1.13
$2N_2$	2.62	1.13	–	–	–	–	2.65	1.14
OO_1	1.13	1.14	–	–	–	–	1.15	1.14
J_1	1.08	1.00	–	–	–	–	1.10	0.94
φ_1	0.77	0.91	–	–	–	–	–	–
ψ_1	1.31	1.15	–	–	–	–	–	–
K_1	23.76	9.42	2.28	2.20	2.62	2.18	2.61	2.17
S_1	3.57	1.81	–	–	–	–	–	–
P_1	4.36	2.04	1.41	1.00	1.39	0.96	1.39	0.96
M_1	1.15	0.89	–	–	–	–	1.14	0.86
O_1	10.43	5.14	1.06	1.20	0.99	1.21	1.00	1.20
ρ_1	1.73	0.85	–	–	–	–	–	–
Q_1	0.85	1.12	0.68	1.05	0.68	1.06	0.67	1.06
Mtm	1.18	1.00	–	–	–	–	1.18	1.00
Mf	1.25	1.49	1.17	1.49	–	–	1.15	1.47
Mm	1.65	1.02	–	–	–	–	1.58	1.06
Ssa	1.67	1.49	–	–	–	–	1.54	1.48
Sa	6.73	3.61	–	–	–	–	6.74	3.61

signal is present also at the second and third harmonics of S_1, we can surmise that it may be caused by some abrupt changes that occur everyday.

[46] The residual signals at other tides are small, but not always negligible. Can they be explained by the uncertainties in ocean loading models? Error analysis for ocean tide models is rather complicated [*Scherneck*, 1993]. As was shown by *Ray et al.* [2001] the root mean square of the differences of several competing ocean models is not an adequate measure of their formal uncertainties. In order to compute standard deviations of ocean loading coefficients, the special set of 29 solutions of the K_1 and M_2 ocean tides model made by *Egbert and Yerofeeva* [2002] (R. Ray, private communication, 2001) was analyzed using a Monte Carlo approach [*Dushaw et al.*, 1997]. This set of models was produced by inversion of synthetic data sets with adding noise due to expected random data errors and Laplace tidal equation forcing errors. For each Monte Carlo realization of the ocean tide model, the displacements due to mass loading were computed for the stations of interest, and the standard deviations of these series of displacements were calculated. This method is frequency independent internally, and the estimated uncertainties for ocean loading at the K_1 and M_2 frequencies can be considered as an adequate measure of the uncertainties of other semidiurnal and diurnal ocean loading models, although an extrapolation to long period tides is not warranted. However, taking into account statistical formal uncertainties of ocean loading reduces χ^2/ndg insignificantly.

[47] In order to evaluate the influence of possible errors in the computation of ocean loading, the ocean loading dis-

placements were computed with different Green's functions, different coastal resolution and with different computer programs (courtesy of H.-G. Scherneck). The differences in ocean loading displacements did not exceed 5% and are less than the differences due to the formal uncertainties of the ocean tide models.

[48] Another possible cause of the discrepancies was investigated: deficiencies of the solid Earth tide model which can affect more strongly the tides near the free core resonance, such as K_1. The residual displacement due to errors in Love numbers should be, first, proportional to the amplitude of the tidal potential for that wave; second, should not depend on station longitude. The field of residual harmonic site position variations is not consistent with these conditions.

4.2. Ocean Loading Models for Minor Tides

[49] Analysis of Table 2 shows that the amplitudes of site position variations at the frequencies of some minor tides statistically significantly differ from zero. Ocean loading computed using the NAO99 model does not reduce χ^2. The NAO99 ocean tide model contains cotidal maps for 8 major diurnal and semidiurnal tides as well as 8 minor tides: T_2, L_2, ν_2, μ_2, $2N_2$, OO_1, J_1, and M_1. These tidal maps were obtained using the response method [*Munk and Cartwright*, 1966], and the ocean tide admittance was modeled by a low-order polynomial across each tidal band. Cotidal maps for minor tides were effectively obtained by interpolating an admittance curve fitted to the major tides. It was assumed that the admittance is a smooth enough function to allow us interpolation across the entire band.

[50] The χ^2 of site position variations for the minor tides is comparable with the χ^2 of residuals of the problematic K_1, K_2 and S_1, S_2 tides, and therefore, is at the same order of magnitude as possible systematic errors of ocean tides model for the major tides. Using observed site position variations, an empirical ocean loading admittance was computed on the assumption that the site displacement are caused entirely by ocean loading. Admittance is defined here as a ratio of the observed site displacement to the amplitude of the tide-generating potential. These values of the admittance for major tides were used to compute interpolation polynomials over the diurnal and semidiurnal band, and the interpolated values of the admittance for minor tides were compared with the actual admittance values. The differences turned out to be comparable with the values of admittance themselves. Thus, measurements of admittance for the major tides do not allow us to predict admittance for minor tides. Presumably, it is not sufficient to have four points per band contaminated by measurement noise and presence of a nontidal signal in order to adequately represent dependence of the admittance on frequency.

[51] Another class of minor tides are close companions of the major tides. Since harmonic site position variations for these tides cannot be reliable obtained, their influence was evaluated indirectly. Another solution called H4 was made. In contrast to the base solution, only the main constituents of each tidal wave were taken into account. Comparison of solutions H1 and H4 showed that dropping close companions increased the wrms of postfit residuals from 23.173 to 23.180 ps and increased χ^2 of residual site position varia-
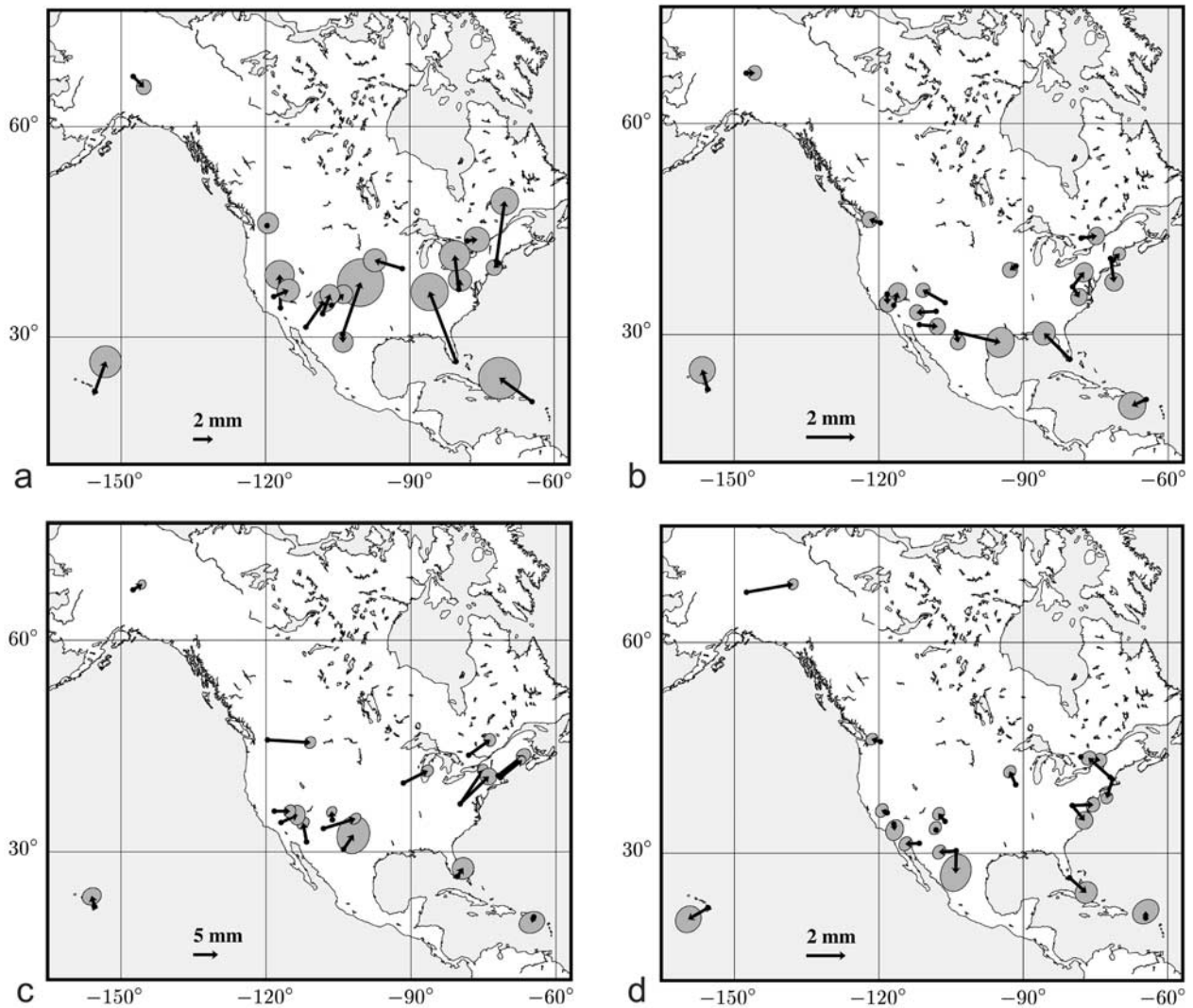
Figure 6. Phasor diagram for diurnal (S_1) and annual site position variations in North America. (a) Up displacements at diurnal frequency. (b) East displacements at diurnal frequency. (c) Up displacements at annual frequency. (d) North displacements at annual frequency. Length of an arrow is proportional to the amplitude of the site harmonic displacement. Direction of the arrow shows the phase lag of the displacement with respect to the astronomical tide. The phases are counted clockwise from the upward direction. Error ellipse corresponds to a rescaled uncertainty of the displacement. Astronomical S_1 tide has a maximum at approximately 13^h local solar time. Astronomical Sa tide has a maximum around 29 June each year.

tions for several tidal waves which have strong companion waves: K_1, O_1, and K_2. Thus, we can conclude that observations confirm the validity of admittance interpolation within a very narrow band.

4.3. Models for Long Period Tides

[52] Applying ocean loading models reduces χ^2 for zonal tides only marginally. The signal itself is much weaker and barely exceeds the significance level at the Mf and Mm frequencies. Ocean tide models for long period tides are less reliable due to the sparseness of long period ocean tide gauge data and difficulties in extracting the ocean tide signal during the process of assimilating altimeter data. The observed sea level changes at the Sa and Ssa frequencies contain a considerable portion of the steric effect that does not cause mass loading.

[53] In order to investigate a possible contribution of hydrological loading due to continental water storage variations, the series of hydrological loading for 1994–1999 computed by *van Dam et al.* [2001] were used. A six-parameter model, average, linear trend, sine and cosine variations with annual and semiannual periods, was fitted. Parameters of harmonic variations due to hydrological loading were added to the coefficients of ocean loading computed using the NAO99 model at the Sa and Ssa waves, and the observed site position variations were checked against the combined model. Table 4 shows that the residual signal at the annual frequency was significantly reduced when the model of hydrological loading was taken into account. At the same time the residuals did not vanish completely. It indicates that either the model of hydrological loading is not precise enough or there is a signal at annual

Table 4. χ^2/ndg Statistic of Residual Harmonic Site Position Variations With Annual and Semiannual Periods After Subtraction of the Ocean and Hydrological Loading Models

	No Model		NAO99		NAO99+ Hydrology	
Wave	Vert	Horz	Vert	Horz	Vert	Horz
Ssa	1.67	1.49	1.54	1.48	1.53	1.54
Sa	6.73	3.61	6.74	3.61	4.62	3.36

and semiannual frequencies other than tidal ocean and hydrological loading.

4.4. Comparison With GPS

[54] *Schenewerk et al.* [2001] derived vertical site position variations at 8 tidal waves for 353 sites using GPS observations in 1997–1999. The GPS data set is shorter than the VLBI data set, but more uniform: all sites observed everyday, every third day was used in the analysis. Amplitudes and phases of only vertical displacements were estimated. The authors of that paper obtained the GPS solution using an approximation: the complete data set was broken into daily subsets which were, in turn, broken into regional subnetworks. Further analysis was done by setting the correlations between these blocks to zero.

[55] 28 out of 40 VLBI sites studied in this paper are collocated within 20 km of a GPS station used in the GPS solution. Real and imaginary parts of harmonic site position variations from this solution were compared with the VLBI results and with the GOT00 ocean loading model. For each collocated site three vector differences, VLBI minus model, GPS minus model, VLBI minus GPS, were formed and the weighted root mean square statistics (wrms) of these differences were calculated. Results of comparison for each wave are presented in Table 5. In addition to that, the wrms of the total observed amplitudes of vertical displacements were computed. Analysis of this table suggests that the displacements derived from GPS have much larger errors than was expected. Since VLBI results are considerably closer to the ocean loading model at these frequencies, and the differences VLBI-GPS and GPS model are comparable, we can conclude that the differences between VLBI and GPS vertical site position variations are almost entirely due to errors in the GPS solution. The largest discrepancy between GPS results and the model is at K_1 and K_2 frequencies, which in the case of K_2 is comparable with the signal itself. These differences are much larger than the VLBI minus model differences and, presumably, have a different origin.

Table 5. WRMS of the Total Amplitudes of Vertical Displacements From GPS and From VLBI, and WRMS of the Residual Amplitudes With Respect to the Ocean Loading Model GOT00

Wave	GPS − VLBI (mm)	GPS Total (mm)	GPS Model (mm)	VLBI Total (mm)	VLBI − Model (mm)
M_2	6.2	13.5	5.4	10.1	0.9
K_2	9.1	8.7	8.9	1.4	1.4
S_2	3.3	5.4	3.3	3.2	1.7
N_2	1.7	2.8	1.3	2.3	1.0
O_1	3.6	6.7	3.3	4.3	1.2
K_1	7.6	11.7	6.9	6.4	2.2
P_1	3.3	3.8	3.1	2.4	1.3
Q_1	1.8	1.7	1.4	1.2	1.1

Table 6. Comparison of the Complex Correlation Coefficient Between the Annual Site Position Variations From VLBI and GPS Analyses

GPS Solution	Mass Loading Applied	Coherence Amplitude	Coherence Phase (rad)
SOPAC	no	0.48	−0.08
SOPAC	yes	0.42	−0.34
JPL	no	0.38	−0.23
JPL	yes	0.31	0.13

[56] Annual vertical site position variations were obtained by *Dong et al.* [2002] from analysis of the continuous GPS array daily solutions generated at the Scripps Orbit and Permanent Array Center (SOPAC) and at the Jet Propulsion Laboratory (JPL) in the 4.5-year period from January 1996 to June 2002. 25 VLBI sites are collocated within 30 km of a GPS station used in these GPS solutions. Complex amplitudes of annual variations of positions of these stations were compared. Complex correlation coefficient ρ defined as

$$\rho = \frac{\sum\limits_{k}^{n} a_k^* b_k}{\sum\limits_{k}^{n} a_k^* a_k \sum\limits_{k}^{n} b_k^* b_k} \qquad (9)$$

was used as a measure of coherency. Here a_k and b_k are standardized complex amplitudes determined from VLBI and GPS observations respectively:

$$a_k = \frac{v_{Rk} - \bar{v}_R}{\sigma_{Rk}} + i\frac{v_{Ik} - \bar{v}_I}{\sigma_{Ik}}$$
$$b_k = \frac{g_{Rk} - \bar{g}_R}{\sigma_{Rk}} + i\frac{g_{Ik} - \bar{g}_I}{\sigma_{Ik}} \qquad (10)$$

A horizontal bar denotes the average value and an asterisk denotes complex conjugation.

[57] Two comparisons were done. In the first test the raw annual site position variations, which included mass loading effects, were compared. The contribution due to pole tide was subtracted from the GPS amplitudes, and the contribution due to atmosphere mass loading computed by *Dong et al.* [2002] was added to the VLBI amplitudes. In the second test the contribution to mass loading due to annual variations of soil moisture, snow and nontidal sea level variations provided by *Dong et al.* [2002] was subtracted from both VLBI and the GPS annual site position variations. In addition to that, the annual variations due to atmosphere loading were subtracted from the GPS annual site position variations. Results are presented in Table 6.

[58] Assuming that the complex amplitudes are normally distributed and uncorrelated, the correlation coefficient is distributed in Student t distribution with 48 degrees of freedom [*Kendall and Stuart*, 1958], and therefore, at 95% probability should not exceed 0.28. Failure of this hypothesis even after applying mass loading shows that there exists a positive correlation at the 5% significant level between the amplitudes of annual site position variations derived from VLBI and from GPS.

4.5. Improvements of Fit

[59] In order to evaluate how significantly estimation of harmonic site position variations improves the fit, two other

Table 7. Statistics of Solutions

Solution	WRMS (ps)	χ^2/ndg
H1	23.06	0.896
R1	23.17	0.904
R2	23.44	0.926

solutions were made: solution R1 without estimating these variations but with an application of the a priori ocean loading model using the coefficients given in the IERS Conventions 1996 [*McCarthy*, 1996], and solution R2 without neither estimating nor using a model of a priori site position variations due to ocean loading. The wrms and χ^2/ndg of postfit residuals are shown in Table 7. The *F* test shows that the reduction of χ^2/ndg for including 7000 new parameters in H1 solution with respect to the R1 and R2 solutions is significant at the 0.1% level.

[60] Another test was to check how the empirical model of site position variations improves the accuracy of results. One of the measures of accuracy is baseline length repeatability. In solution (B1), site positions were estimated for each individual observing session independently, and the empirical model of site position variations extracted from the H1 solution was applied. For each baseline a series of lengths was obtained. A linear model of baseline lengths was fitted to each series, and the wrms of the deviations from the linear model was computed for each baseline. The set of wrms was fitted by a function $\sqrt{A^2 + (B \cdot L)^2}$ where L is the mean baseline length. Coefficients A and B, which represent the average baseline length repeatability, are a measure of accuracy. For comparison purposes solution (B2) applying the IERS96 ocean loading model and solution (B3) applying neither the empirical nor the theoretical ocean loading model were made. The baseline length repeatability was computed for the entire set of baseline lengths and for the restricted set of baseline lengths comprised of only the baselines that are shorter than 9000 km and were observed after 1993.0. Table 8 shows that applying the empirical model of harmonic site position variations improves also accuracy.

[61] Estimation of harmonic site position variations did not improve the agreement of the EOP results obtained at simultaneously running VLBI networks.

5. Conclusion

[62] Analysis of 20 years of VLBI data allowed us to measure harmonic position variations for 40 sites with an accuracy at the submillimeter level for both vertical and horizontal components. Analysis of the displacements at a large number of sites allows us to make certain conclusions of how well our models perform not only for the specific sites of interest but also globally. After removing the contribution of solid Earth tides, the major cause of these displacements at diurnal and semidiurnal bands is ocean loading. Applying contributions due to ocean loading based on modern ocean tide models at 6 major tides significantly reduces the amplitude of the residual signal for both vertical and horizontal components.

[63] VLBI results allow us to distinguish between different models for the M_2 tide. Ocean loading displacements computed on the basis of the models GOT00 or NAO99 are closer to the observed station displacements than the old

Schwiderski model. The difference for other tides is not significant.

[64] At the same time discrepancies between VLBI results and ocean loading models for K_1, S_1, K_2, and S_2 tides exceed both the formal errors of the estimates and the errors of the ocean loading displacements based on reported formal uncertainties of the ocean tide models. The field of residual displacements is not chaotic, but shows a pattern of spatial coherence.

[65] Estimated displacements at the frequencies of minor tides, except close companions of major tides, do not agree with the ocean loading obtained by interpolation of admittances from major tides. Either the dynamics of the ocean is more complicated and a simple model of smooth interpolation is not applicable, or the errors of interpolation are significant and comparable with the signal. The validity of the recommendation of IERS Conventions 1996 [*McCarthy*, 1996] to use a polynomial interpolation of ocean loading coefficients across the band for all minor tides was not confirmed. However, propagation of the ocean tide model to close companions of the major tides for computation of displacements due to ocean loading through admittance relations is warranted and VLBI observations confirm it.

[66] Displacements at the frequencies of zonal tides are only partly coherent with ocean loading models. The signal at the annual frequency is not due to tides. Applying the hydrological loading model significantly reduces the residual signal, but does not eliminate it entirely.

[67] It is remarkable that the annual site position variations derived from VLBI correlate with the variations derived from GPS after removal of mass loading effects at the 5% confidence level. It strongly supports an assertion that this signal is not a VLBI-specific artifact but a manifestation of either mismodeled annual crust deformations or systematic errors common for VLBI and GPS, such as errors in modeling troposphere path delay.

[68] Applying an empirical model of harmonic site position variations to VLBI processing improves both precision and accuracy: it statistically significantly reduces the fit and improves the baseline length repeatability with respect to using theoretical models of harmonic site displacements. Thus, the technology of space geodesy has surpassed our ability to predict harmonic site position variations. New refinements of ocean tide and hydrology models are needed to explain the empirical results.

Appendix A: Algorithm for the Computation of Displacements Due to Solid Earth Tide of the Second Degree

[69] *Mathews et al.* [1995] proposed the following formalism for the representation of a displacement field caused by the solid Earth tides of the second degree:

Table 8. Baseline Length Repeatability

Solution	All Data		1993–2001	
	A (mm)	B	A (mm)	B
B1	1.7	1.6×10^{-9}	1.6	1.0×10^{-9}
B2	2.1	1.7×10^{-9}	2.1	1.2×10^{-9}
B3	2.2	1.8×10^{-9}	2.2	1.2×10^{-9}

$$\vec{d}_{\text{REN}} = \sum_{m=0}^{m=2} \frac{\Phi_2^m a_e^2}{g_e} \left[\left(h^{(0)} + h^{(2)} P_2^0 \right) \mathbf{R}_2^m + h' \mathbf{R}_0^m \right.$$

$$\left. + \left(l^{(0)} + l^{(2)} P_2^0 \right) \mathbf{S}_2^m + l^{(1)} P_1^0 \mathbf{T}_2^m + l' \mathbf{T}_1^m \right] \quad \text{(A1)}$$

where Φ_2^m is the tidal potential of the second degree and R, S, and T denote radial, transverse spheroidal, and toroidal vector harmonic fields:

$$\mathbf{R}_\ell^m = \vec{r} Y_\ell^m \qquad \mathbf{S}_\ell^m = r \nabla Y_\ell^m \qquad \mathbf{T}_\ell^m = i\, \vec{r} \times \nabla Y_\ell^m \quad \text{(A2)}$$

here $\vec{r}$ is a unit station coordinate vector, Y_ℓ^m is a spherical harmonic function of degree ℓ and order m normalized over the unit sphere, a_e is the Earth's equatorial radius, g_e is the gravity acceleration at the equator, P_ℓ^m is a Legendre function, and h and l are the generalized Love numbers:

$h^{(0)}$ and principal Love number
$h^{(i)}$ out-of-phase radial Love number
$h^{(2)}$ latitude Love number
h' zero-degree Love number
$l^{(0)}$ principal Shida number
$l^{(i)}$ out-of-phase Shida number
$l^{(1)}$ second-degree toroidal Love number
$l^{(2)}$ latitude Shida number
l' first-degree toroidal Love number

[70] In order to transform (A1) to the form suitable for computations we do the following operations: (1) substitute direct expressions for vector harmonic fields (A2); (2) add out-of-phase terms; (3) expand the tidal potential in a Fourier time series; and (4) separate the terms which depend on station latitude and longitude from the terms which depend on time. After some algebra we get the following expression for a tidal displacement vector $\vec{d}_{\text{ren}}$ with radial, east and north components:

$$\vec{d}_{\text{REN}} =$$

$$\sum_{m=0}^{m=2} \begin{bmatrix} \vec{X}_1^{rc}(m,\varphi) \cdot \sum_{k=1}^{n(m)} A_k \vec{L}_1^r(k) \cos\gamma_{km} - \vec{X}_1^{rs}(m,\varphi) \cdot \sum_{k=1}^{n(m)} A_k \vec{L}_1^r(k) \sin\gamma_{km} \\ \vec{X}_2^{rc}(m,\varphi) \cdot \sum_{k=1}^{n(m)} A_k \vec{L}_2^r(k) \sin\gamma_{km} + \vec{X}_2^{rs}(m,\varphi) \cdot \sum_{k=1}^{n(m)} A_k \vec{L}_2^r(k) \cos\gamma_{km} \\ \vec{X}_3^{rc}(m,\varphi) \cdot \sum_{k=1}^{n(m)} A_k \vec{L}_3^r(k) \cos\gamma_{km} - \vec{X}_3^{rs}(m,\varphi) \cdot \sum_{k=1}^{n(m)} A_k \vec{L}_3^r(k) \sin\gamma_{km} \end{bmatrix}$$

$$+ \sum_{m=0}^{m=2} \begin{bmatrix} -\vec{X}_1^{ic}(m,\varphi) \cdot \sum_{k=1}^{n(m)} A_k \vec{L}_1^i(k) \sin\gamma_{km} - \vec{X}_1^{is}(m,\varphi) \cdot \sum_{k=1}^{n(m)} A_k \vec{L}_1^i(k) \cos\gamma_{km} \\ \vec{X}_2^{ic}(m,\varphi) \cdot \sum_{k=1}^{n(m)} A_k \vec{L}_2^i(k) \cos\gamma_{km} - \vec{X}_2^{is}(m,\varphi) \cdot \sum_{k=1}^{n(m)} A_k \vec{L}_2^i(k) \sin\gamma_{km} \\ -\vec{X}_3^{ic}(m,\varphi) \cdot \sum_{k=1}^{n(m)} A_k \vec{L}_3^i(k) \sin\gamma_{km} - \vec{X}_3^{is}(m,\varphi) \cdot \sum_{k=1}^{n(m)} A_k \vec{L}_3^i(k) \cos\gamma_{km} \end{bmatrix}$$

$$\text{(A3)}$$

where vector $\vec{X}$ depends only on station coordinates:

$$\begin{aligned} \vec{X}_j^{rc}(m,\varphi) &= \vec{Z}_j^r(m,\varphi) \cdot \cos m\lambda \\ \vec{X}_j^{rs}(m,\varphi) &= \vec{Z}_j^r(m,\varphi) \cdot \sin m\lambda \\ \vec{X}_j^{ic}(m,\varphi) &= \vec{Z}_j^i(m,\varphi) \cdot \cos m\lambda \\ \vec{X}_j^{is}(m,\varphi) &= \vec{Z}_j^i(m,\varphi) \cdot \sin m\lambda \end{aligned} \quad \text{(A4)}$$

here φ is geocentric latitude and λ is positive towards east longitude. Vector $\vec{Z}$ is

$$\vec{Z}_1^r = \begin{pmatrix} \bar{P}_2^m \frac{1}{g_e} \\ P_2^0 \bar{P}_2^m \frac{1}{g_e} \\ 0 \\ \frac{1}{g_e} \end{pmatrix} \qquad \vec{Z}_1^i = \left(\bar{P}_2^m \frac{1}{g_e} \right)$$

$$\vec{Z}_2^r = \begin{pmatrix} -\frac{m}{\cos\varphi} \bar{P}_2^m \frac{1}{g_e} \\ -\frac{m}{\cos\varphi} P_2^0 \bar{P}_2^m \frac{1}{g_e} \\ P_1^0 \frac{\partial \bar{P}_2^m}{\partial\varphi} \frac{1}{g_e} \\ \frac{\partial \bar{P}_1^m}{\varphi} \frac{1}{g_e} \end{pmatrix} \qquad \vec{Z}_2^i = \left(-\frac{m}{\cos\varphi} \bar{P}_2^m \frac{1}{g_e} \right) \quad \text{(A5)}$$

$$\vec{Z}_3^r = \begin{pmatrix} \frac{\partial \bar{P}_2^m}{\partial\varphi} \frac{1}{g_e} \\ P_2^0 \frac{\partial \bar{P}_2^m}{\partial\varphi} \frac{1}{g_e} \\ -\frac{m}{\cos\varphi} P_1^0 \bar{P}_2^m \frac{1}{g_e} \\ -\frac{m}{\cos\varphi} \bar{P}_1^m \frac{1}{g_e} \end{pmatrix} \qquad \vec{Z}_3^i = \left(\frac{\partial \bar{P}_2^m}{\partial\varphi} \frac{1}{g_e} \right)$$

P_m^0 is a Legendre function normalized to have maximal value 1:

$$\begin{aligned} P_1^0 &= \sin\varphi & P_1^1 &= \cos\varphi & P_1^2 &= 0 \\ P_2^0 &= \left(\tfrac{3}{2}\sin^2\varphi - \tfrac{1}{2} \right) & P_2^1 &= 2\sin\varphi\cos\varphi & P_2^2 &= \cos^2\varphi \end{aligned} \quad \text{(A6)}$$

and $\bar{P}_l^m$ are Legendre functions normalized over the surface of the unit sphere:

$$\begin{aligned} \bar{P}_1^0 &= P_1^0 & \bar{P}_1^1 &= P_1^1 & \bar{P}_1^2 &= P_1^2 \\ \bar{P}_2^0 &= \sqrt{\tfrac{5}{4\pi}} P_2^0 & \bar{P}_2^1 &= \sqrt{\tfrac{15}{32\pi}} P_2^1 & \bar{P}_2^2 &= \sqrt{\tfrac{15}{32\pi}} P_2^2 \end{aligned} \quad \text{(A7)}$$

g_e is the Earth's equatorial gravity acceleration.

[71] The summing in (A3) is done over the constituents of the spectral expansion of the tide-generating potential that is assumed to be in the form

$$\Phi_2^m(t,r) = \sum_{m=0}^{m=2} \left(\frac{r}{a_e} \right)^2 \bar{P}_2^m(\varphi) \cdot \sum_{k=1}^{n(m)} A_k \cdot \cos\gamma_{km} \quad \text{(A8)}$$

where r is the distance from the geocenter, a_e is the semimajor axis of the Earth, A_k is the normalized amplitude of the kth tidal wave and γ_{km} is its argument:

$$\gamma_{km} = \psi_k + \theta_k + \omega_k t_{\text{TDB}} + m \frac{2\pi(\text{UT1} - t_{\text{TDB}})}{86400} \quad \text{(A9)}$$

ψ_k is the phase of the kth wave, θ_k and ω_k are the phase and frequency of the harmonic argument of that wave. t_{TDB} is the time elapsed since the fundamental epoch J2000.0 (12^h 1 January 2000) at the TDB scale. The difference UT1 − t_{tdb} in (A9) takes into account variations in the Earth's rotation which were omitted in producing the tidal potential series. The variable m = 0,1,2 in (A3)–(A5) denotes the order of a tidal wave, subscript index 1, 2, and 3 denotes component of the displacement vector: radial, east, north, and summation is carried out over spectral harmonics of the tidal expansion. The number of constituents in sum (A8), $n(m)$, is determined by a truncation level.

[72] The vector of generalized Love numbers is presented in the form

$$\vec{L}_1^r = \left(h^{(0)}, h^{(2)}, 0, h'\right)^\top \qquad \vec{L}_1^i = h^{(i)}$$

$$\vec{L}_2^r = \left(l^{(0)}, l^{(2)}, l^{(1)}, l'\right)^\top \qquad \vec{L}_2^i = l^{(i)} \qquad \text{(A10)}$$

$$\vec{L}_3^r = \left(l^{(0)}, l^{(2)}, l^{(1)}, l'\right)^\top \qquad \vec{L}_3^i = l^{(i)}$$

[73] All generalized Love numbers are considered to be complex and frequency-dependent. The generalized Love numbers are computed according to the analytical expressions presented by *Mathews* [2001] with corrections for some specific tidal waves taken from the tables.

[74] The advantages of this scheme are that the sums like $\sum A_k \vec{L}_1^r(k) \sin \gamma_{km}$ depend only on time and do not depend on station coordinates, and therefore, may be used for the calculation of displacements of many stations at the same epoch. The vectors $\vec{X}$ do not depend on time and are computed only once.

[75] The HW95 expansion contains sine and cosine coefficients C_0 and S_0. Having these coefficients, we can compute phases and amplitudes for (A3) as $\psi_k = -\arctan \frac{S_{0k}}{C_{0k}}$ and $A_k^m = \rho(m)\sqrt{C_{0k}^2 + S_{0k}^2}$, where $\rho(m)$ is a renormalization factor. It is $\sqrt{4\pi}$ for tides of the 0th order and $\sqrt{8\pi}$ for other tides.

[76] Frequencies and phases of tidal constituents are easily computed via coefficients at fundamental arguments.

$$\theta_i = \sum_{j=1}^{j=11} k_{ij} F_{jo} + \theta_{ai}$$

$$\text{(A11)}$$

$$\omega_i = \sum_{j=1}^{j=11} k_{ij} F_{j1} + \omega_{ai}$$

where F_{jq} are fundamental coefficients from the theory of planetary motion [*Simon et al.*, 1994]. We neglected terms of the second degree and higher.

Appendix B: Algorithm for the Computation of Displacements Due to Solid Earth Tides of the Third Degree

[77] For computation of displacements due to solid Earth tides of the third degree with a precision of 0.1mm we can neglect frequency dependence of Love numbers and an admixture of terms in tide-generating potential other than third degree as well as out-of-phase Love numbers. Therefore, vector of displacements can be written in the form

$$\vec{d}_{\text{REN}} = \sum_{m=0}^{m=3} \begin{pmatrix} X_1^{3c}(m,\varphi)h_3 \cdot \sum_{k=1}^{n(m)} A_k \cos \gamma_{km} - X_1^{3s}(m,\varphi)h_3 \cdot \sum_{k=1}^{n(m)} A_k \sin \gamma_{km} \\ X_2^{3c}(m,\varphi)l_3 \cdot \sum_{k=1}^{n(m)} A_k \sin \gamma_{km} + X_2^{3c}(m,\varphi)l_3 \cdot \sum_{k=1}^{n(m)} A_k \cos \gamma_{km} \\ X_3^{3c}(m,\varphi)l_3 \cdot \sum_{k=1}^{n(m)} A_k \cos \gamma_{km} - X_s^{3s}(m,\varphi)l_3 \cdot \sum_{k=1}^{n(m)} A_k \sin \gamma_{km} \end{pmatrix}$$

$$\text{(B1)}$$

where X depends only on station coordinates in the following way:

$$X_j^{3c}(m,\varphi) = Z_j^3(m,\varphi) \cdot \cos m\lambda$$

$$X_j^{3s}(m,\varphi) = Z_j^3(m,\varphi) \cdot \sin m\lambda$$

here Z_j^3 is

$$Z_1^3(m,\varphi) = \bar{P}_3^m \frac{1}{g_e}$$

$$Z_2^3(m,\varphi) = -\frac{m}{\cos \varphi} \bar{P}_3^m \frac{1}{g_e} \qquad \text{(B2)}$$

$$Z_3^3(m,\varphi) = \frac{\partial \bar{P}_3^m}{\partial \varphi} \frac{1}{g_e}$$

[78] Legendre functions of third order are

$$P_3^0 = \left(\frac{5}{2} \sin^3 \varphi - \frac{3}{2} \sin \varphi\right)$$

$$P_3^1 = \left(\frac{5}{2} \sin^2 \varphi - \frac{1}{2} \sin \varphi\right) \cos \varphi$$

$$P_3^2 = \sin \varphi \cos^2 \varphi \qquad \text{(B3)}$$

$$P_3^3 = \cos^3 \varphi$$

$$\bar{P}_3^0 = \sqrt{\frac{7}{4\pi}} P_3^0 \qquad \bar{P}_3^1 = \sqrt{\frac{21}{16\pi}} P_3^1$$

$$\bar{P}_3^2 = \sqrt{\frac{105}{32\pi}} P_3^2 \qquad \bar{P}_3^3 = \sqrt{\frac{35}{64\pi}} P_3^3 \qquad \text{(B4)}$$

[79] Analogously to the tides of the second degree, the amplitudes of the tide-generating potential produced from the HW95 expansion should be multiplied by the same renormalization factors.

[80] Software for computation of site displacements due to solid Earth tides of the second and third degree is available on the Web at http://gemini.gsfc.nasa.gov/sotid.

References

Agnew, D. C., *SPOTL: Some Programs for Ocean-Tide Loading, SIO Ref. Ser.*, vol. 96–9, 35 pp., Scripps Inst. of Oceanogr., La Jolla, Calif., 1996.

Agnew, D. C., NLOADF: A program for computing ocean-tide loading, *J. Geophys. Res.*, 102, 5109–5110, 1997.

Buellesfeld, H., and H. Schuh, New harmonic development of the tide-generating potential, ETMB85, with application on VLBI data analysis, in *Proceedings of the 10th Symposium on Earth Tides, Madrid*, edited by R. Vieira, pp. 933–942, Cons. Super. de Invest. Cient., Madrid, 1986.

Clark, T. A., et al., Precision geodesy using the MARK-III very long baseline interferometric systems, *IEEE Trans. Geosci. Remote Sens.*, 25(4), 438–449, 1985.

Christodoulidis, D. C., D. E. Smith, S. M. Kosko, and P. J. Dunn, Solid Earth and ocean tides parameters from LAGEOS, in *Proceedings of the 10th Symposium on Earth Tides, Madrid*, edited by R. Vieira, pp. 953–961, Cons. Super. de Invest. Cient., Madrid, 1986.

Dong, D., P. Fang, Y. Bock, M. K. Cheng, and S. Miyazaki, Anatomy of apparent seasonal variations from GPS derived site position time series, *J. Geophys. Res.*, 107, 10.1029/2001JB000573, 2002.

Dragert, H., T. S. James, and A. Lambert, Ocean loading corrections for continuous GPS: A case study at the Canadian coastal site Holberg, *Geophys. Res. Lett.*, 27, 2045–2048, 2000.

Dushaw, B. D., G. D. Egbert, P. T. Worchester, B. D. Cornuelle, B. M. Howe, and K. Metger, A TOPEX/POSEIDON global tidal model (TPXO.2) and barotropic tidal currents determined from long-range acoustic transmissions, *Prog. Oceanogr.*, 40, 337–367, 1997.

Egbert, G. D., and S. Y. Erofeeva, Efficient inverse modeling of barotropic tides, *J. Atmos. Oceanic Technol.*, 19(2), 183–204, 2002.

Farell, W. E., Deformation of the Earth by surface loads, *Rev. Geophys. Space Phys.*, 10, 761–797, 1972.

Gendt, G., and R. Dietrich, Geometrical tidal effects from LAGEOS laser ranging data, in *Proceedings of the 10th Symposium on Earth Tides, Madrid*, edited by R. Vieira, pp. 963–968, Cons. Super. de Invest. Cient., Madrid, 1986.

Gipson, J., Very long baseline interferometry determination of neglected tidal terms in high-frequency Earth orientation variation, *J. Geophys. Res.*, 101, 28,051–28,064, 1996.

Haas, R., and H. Schuh, Determination of frequency dependent Love and Shida numbers from VLBI data, *Geophys. Res. Lett.*, 23, 1509–1512, 1996.

Haas, R., and H. Schuh, Ocean loading observed by geodetic VLBI, in *Proceeding of the 13th International Symposium on Earth Tides*, edited by B. Ducarme and P. Paquet, pp. 111–120, 1998.

Hartmann, T., and H.-G. Wenzel, The HW95 tidal potential catalogue, *Geophys. Res. Lett.*, 22, 3353–3356, 1995.

Hatanaka, Y., A. Sengoku, T. Sato, J. M. Johnson, C. Rocken, and C. Meertens, Detection of tidal loading signals from GPS permanent array of GSI Japan, *J. Geod. Soc. Jpn.*, 47(1), 187–192, 2001.

Herring, T. A., et al., Determination of tidal parameters from VLBI observations, in *Proceedings of the IX International Symposium on Earth Tides, Stuttgart*, edited by R. Viera, pp. 205–214, 1983.

Kendall, M. G., and A. Stuart, *The Advanced Theory of Statistics*, Charles Griffin, London, 1958.

Lambert, A., S. D. Pagiatakis, A. P. Billyard, and H. Dragert, Improved ocean tide loading corrections for gravity and displacements: Canada and northern United States, *J. Geophys. Res.*, 103, 30,231–30,244, 1998.

MacMillan, D. S., and J. M. Gipson, Atmospheric pressure loading parameters from very long baseline interferometric observations, *J. Geophys. Res.*, 99, 18,081–18,087, 1994.

MacMillan, D. S., and C. Ma, Evaluation of very long baseline interferometry atmospheric modeling improvements, *J. Geophys. Res.*, 99, 637–651, 1994.

MacMillan, D. S., and C. Ma, Improvement of VLBI EOP accuracy and precision, in *IVS 2000 General Meeting Proceedings, Greenbelt*, edited by N. Vandenberg and K. Baver, pp. 247–251, 2000.

Mathews, P. M., Love numbers and gravimetric factor for diurnal tides, *J. Geod. Soc. Jpn.*, 47(1), 231–236, 2001.

Mathews, P. M., B. A. Buffett, and I. I. Shapiro, Love numbers for a rotating spheroidal Earth: New definitions and numerical values, *Geophys. Res. Lett.*, 22, 579–582, 1995.

Mathews, P. M., V. Dehant, and J. M. Gipson, Tidal station displacements, *J. Geophys. Res.*, 102, 20,469–20,477, 1997.

Matsumoto, K., T. Takanezawa, and M. Ooe, Ocean tide models developed by assimilating TOPEX/POSEIDON altimeter data into hydrodynamical model: A global model and a regional model around Japan, *J. Oceanogr.*, 56, 567–581, 2000.

McCarthy, D. D., IERS Conventions 1996, *IERS Tech. Note*, 21, Paris, 1996.

Mitrovica, J. X., J. L. Davis, P. M. Mathews, and I. I. Shapiro, Determination of tidal h Love number in the diurnal band using extensive VLBI data set, *Geophys. Res. Lett.*, 21, 705–708, 1994.

Munk, W. H., and D. E. Cartwright, Tidal spectroscopy and prediction, *Philos. Trans. R. Soc. London, Ser. A*, 259, 533–581, 1966.

Newcomb, S., On the dynamics of the Earth's rotation, with respect to periodic variations of latitude, *Mon. Not. R. Astron. Soc.*, 52, 336–341, 1892.

Nothnagel, A., Investigations of thermal height changes of geodetic VLBI radio telescopes, in *Proceedings of the 10th Working Meeting on European VLBI for Geodesy and Astrometry*, edited by R. Lanotte and G. Bianco, pp. 121–133, Agenzia Spatiale Ital., Matera, 1995.

Petrov, L., O. Volvach, and N. Nesterov, Measurements of horizontal motion of the station Simeiz using VLBI, *Kinemat. Phys. Celest. Bodies*, 17(5), 424–436, 2001.

Ray, R. D., A global ocean tide model from TOPEX/POSEIDON Altimetry: GOT99.2, *NASA/TM-1999-209478*, Greenbelt, 58 pp., 1999.

Ray, R. D., S. Bettadpur, R. J. Eanes, and E. J. O. Shrama, Geometrical determination of the Love number h_2 at four tidal frequencies, *Geophys. Res. Lett.*, 22, 2175–2178, 1995.

Ray, R. D., R. J. Eanes, G. D. Egbert, and N. K. Pavlis, Error spectrum for the global M_2 ocean tide, *Geophys. Res. Lett.*, 28, 21–24, 2001.

Rothacher, M., G. Beutler, R. Weber, and J. Hefty, High-frequency variations in Earth rotation from Global Positioning System data, *J. Geophys. Res.*, 106, 13,711–13,738, 2001.

Ryan, J. W., et al., Geodesy by radiointerferometry: Determinations of baseline vectors, Earth rotation and solid Earth tide with the Mark-I very long baseline interferometry system, *J. Geophys. Res.*, 91, 1935–1946, 1986.

Ryan, J. W., T. A. Clark, C. Ma, D. Gordon, D. S. Caprette, and W. E. Himwich, Global scale tectonic plate motions measured with CDP VLBI data, in *Contributions of Space Geodesy to Geodynamics: Crustal Dynamics, Geodyn. Ser.*, vol. 23, edited by D. E. Smith and D. L. Turcotte, pp. 37–50, AGU, Washington, D.C., 1993.

Schenewerk, M. S., J. Marshall, and W. Dillinger, Vertical ocean-loading deformations derived from a global GPS network, *J. Geod. Soc. Jpn.*, 47(1), 237–242, 2001.

Scherneck, H.-G., Ocean tide loading: Propagation of errors from the ocean tide into loading coefficients, *Manuscr. Geod.*, 18, 59–71, 1993.

Scherneck, H. G., R. Haas, and A. Laudati, Ocean loading for, in and from VLBI, in *IVS 2000 General Meeting Proceedings, Greenbelt*, edited by N. Vandenberg and K. Baver, pp. 257–262, 2000.

Schuh, H., and L. Moehlmann, Ocean loading station displacements observed by VLBI, *Geophys. Res. Lett.*, 16, 1105–1108, 1989.

Schwiderski, E. W., On charting global ocean tides, *Rev. Geophys. Space Phys.*, 18, 243–268, 1980.

Simon, J. L., P. Bretagnon, J. Chapront, M. Chapront-Touze, G. Francou, and J. Laskar, Numerical expressions for precession formulae and mean elements for the Moon and the planets, *Astron. Astrophys.*, 282, 663–684, 1994.

Sovers, O. J., Vertical ocean loading amplitudes from VLBI measurements, *Geophys. Res. Lett.*, 21, 357–360, 1994.

Sovers, O. J., J. L. Fanselow, and C. S. Jacobs, Astrometry and geodesy with radio interferometry: Experiments, models, results, *Rev. Mod. Phys.*, 70(4), 1393–1454, 1998.

Takahashi, F., T. Kondo, Y. Takahashi, and Y. Koyama, *Very Long Baseline Interferometer*, 243 pp., Ohmsha Ltd., Tokyo, 2000.

Takanezawa, T., K. Matsumoto, M. Ooe, and I. Naito, Effects of long-period ocean tides and crustal deformation predicted by global barotropic model: Periods from Mtm to Sa, *J. Geod. Soc. Jpn.*, 47(1), 545–557, 2001.

Titov, O. A., and H. G. Yakovleva, Seasonal variations in radial components of VLBI stations, *Astron. Astrophys. Trans.*, 18, 593–606, 1999.

van Dam, T. M., and T. A. Herring, Detection of atmospheric pressure loading using very long baseline interferometry measurements, *J. Geophys. Res.*, 99, 4505–4518, 1994.

van Dam, T. M., and J. Wahr, Displacements of the Earth's surface due to atmospheric loading: Effects on gravity and baseline measurements, *J. Geophys. Res.*, 92, 1281–1286, 1987.

van Dam, T. M., G. Blewitt, and M. Heflin, Detection of atmospheric pressure loading using the Global Positioning System, *J. Geophys. Res.*, 99, 23,939–23,950, 1994.

van Dam, T. M., J. Wahr, P. C. D. Millly, A. B. Shmakin, G. Blewitt, D. Lavallee, and K. M. Larson, Crustal displacements due to continental water loading, *J. Geophys. Res.*, *28*, 651–654, 2001.

Vandenberg, N., (Ed.), International VLBI Service for Geodesy and Astrometry, 1999 annual report, *NASA/TP-1999-209243*, 308 pp., NASA, Greenbelt, Md., 1999.

Wu, B., P. B. Y. Zhu, and H. Hsu, Determination of Love numbers using satellite laser ranging, *J. Geod. Soc. Jpn.*, *47*(1), 174–180, 2001.

Zernecke, R., Seasonal variations in height demonstrated at the radiotelescope reference point, in *Proceedings of the 13th Working Meeting on European VLBI for Geodesy and Astrometry, Viechtach*, edited by W. Schlueter and H. Hase, pp. 15–18, 1999.

―――――――――――――

C. Ma, Code 926, NASA Goddard Space Flight Center, Greenbelt, MD 20771, USA. (cma@virgo.gsfc.nasa.gov)

L. Petrov, Code 926, NVI Inc./NASA Goddard Space Flight Center, Greenbelt, MD 20771, USA. (pet@leo.gsfc.nasa.gov)